Spectrum Diagnostics of a Damaged Differential Planetary Gear during Various Operating Conditions

ABSTRACT

Planetary gears are more compact and efficient as power transmissions than fixed-axis gear trains but exhibit more complicated dynamics due to the nonlinear combination of backlash and tooth defects. The majority of current publications are based on theoretical models of ideal planetary gears, and therefore cannot simulate the time varying dynamic forces induced by damaged teeth. By utilizing a multi-body dynamics and motion analysis software, this paper presents unpublished vibration spectra and fault indicators of a ubiquitous multi-input industrial differential planetary design that includes tooth damage. Backlash between the sun and planet gears are precisely dimensioned to avoid teeth interference and undercut. The region of point-to-point contact along the involute profile is modeled elastically and accounts for tooth flexibility. Boundary conditions that closely match realistic operation are considered, including component constraints, resistive bearing torques, and direct modification of the software parametric resolution. Torsional vibration induced by backlash and tooth geometry errors is shown to cause teeth separation and double-sided impacts in unloaded and lightly loaded gearing drives. Frequency analyses reveal distinct sideband modulations of the gear mesh along with sub and super harmonics. The sideband components, which comprise a large portion of the vibration, are used as fatigue diagnostics by identifying the location of manufacturing errors. Additionally, a joint time-frequency analysis (JTFA) is applied to transient start-up conditions that illustrates an oscillating spectrum in which contact forces increase during acceleration. To the best of our knowledge no research results have been published in fault detection of planetary gears using JTFA.

Keywords: Vibration health monitoring, malfunction diagnostics, contact forces, numerical simulation, planetary gear, epicyclic transmission, backlash, chipped tooth, multi-body kinematic model, joint time-frequency analysis.

1. Introduction

The planetary gear train is widely used in transmission design of automobiles, helicopters and aircraft engines due to the numerous advantages over traditional fixed-axis gear transmissions. Since the load being transmitted is shared between several planets, torque capability is significantly increased. One notable advantage of a planetary gear is its distinctive combination of both compactness and magnificent power transmission efficiencies. Despite the above advantages, however, the complicated dynamic forces existing among sun, planet and ring gears are difficult to analyze for the main sources of vibration. Reasonably simulating the practical dynamic force between single-mating-gear pair still remains as an important topic. Needless to say, it is even more challenging to realistically model a planetary gear train with multiple meshing stages. As a result, the dynamic analyses of planetary gear trains have received far less attention than fixed-axis gear trains.

The earliest review papers that discuss the numerical modeling of gear dynamics focus on spur gears: Özgüven and Houser in 1988 [1] and by Parey and Tandon in 2003 [2]. The models had a limited number of degrees of freedom and most commonly did not include tooth defects. Tooth meshing stiffness was characterized as either an average or piecewise linear variation instead of the highly nonlinear Hertzian contact. Parey and Tandon's review included spur gear defects. Parey etc. [3] developed a six DOF nonlinear model for a pair of spur gears on two shafts, calculated the Hertzian stiffness for the tooth surface contact, and implemented the empirical mode decomposition (EMD) method to simulate the different defect widths. The above research is based on fix-axis gears.

Lin and Parker [4] analytically investigate the parametric instability of planetary gears induced by gear mesh stiffness variation. The authors use rectangular waveforms with different contact ratios and mesh phasing to simulate the gear mesh stiffnesses existing between sun-planet and planet-ring gear mating pairs. Instability boundaries are directly associated with meshing parameters in the vibration modes. The authors also demonstrate some numerical simulation results about the teeth separation caused by parametric instability and strong impact in the system response. Lin and Parker [5] derive a theoretical model and carefully identify the important characteristics of the natural frequencies and vibration modes for planetary gears. The model uses three planar degrees of freedom for each component of the planetary gears and takes gyroscopic effects and time-varying gear mesh stiffnesses into consideration. The authors do comprehensive investigations about the distinctive characteristics of each type of mode. Based on the model of reference [5], Guo and Parker [6] extend the two-dimensional lumped-parameter model by incorporating the factors of teeth separation, back-side contact, tooth wedging, and bearing clearances. By scrutinizing the dynamic response of an example planetary gear, the authors investigate the nonlinear tooth wedging behavior often observed on a wind turbine planetary gear train. More research about dynamic behavior of planetary gears can be found in reference [7, 8]. Unfortunately, majority of current papers about planetary gears does not include the interactive effects of backlash and gear teeth damage.

Although a simplified model for even a pair of gears involves sophisticated mathematics, it cannot accurately simulate the gear train's practical dynamic behavior even for an ideal system by simply assuming time-varying gear mesh stiffness as square waveforms. The impact forces between the mating pairs are very sensitive to the geometric profile of gear tooth and the gear backlash which must be carefully designed. Geometric simplifications can be overcome by combining CAD models with ADAMS. Kong and Meagher etc. [9] model the nonlinear contact mechanics of a large gearbox without backlash. Since the authors accurately design the gear profiles using CAD software and carefully choose simulation parameters in ADAMS, some interesting results of the dynamic forces are observed. Sommer and Meagher etc. [14] illustrate the transient and steady state dynamic loading on teeth within a two stage gear transmission arising from backlash and geometric manufacturing errors by utilizing a non-linear multi-body dynamics software model. Vibration and impact force distinctions between backlash and combinations of transmission errors are demonstrated under different initial velocities and load conditions. The backlash and manufacturing errors in the first stage of the gear train are distinct from those of the second stage. By analyzing the signal at a location between the two stages, the mutually affected impact forces are observed from different gear pairs, a phenomenon not observed from single pair of gears. This paper also shows some interesting results about side-band modulations as well as harmonics of the gear mesh frequency. A joint time-frequency response analysis of the fixed-axis gears during start-up illustrates the manner in which contact forces increase during acceleration.

Planetary gear trains can be more compact and efficient as power transmissions than fixed axis gear trains but are also more complicated and less understood in terms of vibration health monitoring. The lack of experimental results about the complicated dynamics of planetary gears and the availability of powerful multi-body dynamics software ADAMS inspire the authors to present this investigation. Some of our initial time-domain results about the differential gear have been published in the conference paper [15]. Based on our recent publications [14] and [15], we have extended and enhanced our research about the differential planetary gear by incorporating frequency analysis and JTFA in this paper. A practical differential planetary gear train with two inputs and one output is studied using multi-body dynamics software. The backlash between the sun gear and planet gears are carefully designed and calculated to avoid teeth interference and undercut. Tooth profile errors are introduced for comparison to ideal gears. The nonlinear contact mechanics model of the meshing teeth is built by careful calculation and selection of the contact simulation parameters such as the stiffness, force exponent, and damping and friction coefficients. Time domain results will show that the dynamic responses due to the combination of backlash and tooth defects depend on the interaction of many components of the differential planetary system. The non-linear factors such as periodically varying mesh stiffness due to alternating tooth contact conditions, backlash, and tooth profile errors are all intrinsically incorporated into the ADAMS software. The dynamics of a differential planetary gear show a rich spectrum of nonlinear phenomena. Frequency analysis shows the appearance of side band modulations as well as harmonics of the gear mesh frequency. In the last part of the paper, the authors demonstrate interesting results about how the frequency contents of the contact force evolve over time using a joint time-frequency analysis based on transient start-up conditions. This research provides a foundation for future vibration-based diagnosis of planetary gears with damaged teeth.

2. Validating a multi-body kinematic formulation for a one-stage gear train

Due to lack of experimental data the multi-body kinematic model has been validated using the published results of [16]. A pair of meshing gear parameters and ADAMS contact parameters are shown in Table 1. The gears are rigid with contact surfaces defined with a penalty based non-linear contact formulation. The non-linear contact force, $F = K(d)^e - cv$, is a vector quantity composed of an elastic and damping portion [10], where d is the penetration depth. The damping force, cv, is proportional to impact velocity, v.

The stiffness coefficient, K, is taken to be the average value of stiffness over one tooth mesh cycle. The force exponent, e, was determined from trial simulations. The damping coefficient generally takes a numeric value between 0.1% - 1% of K. The determination of force exponents however is not obvious and must be based on experience. The ADAMS impact algorithm was chosen as the contact model because of its robustness in numerical integration. The restitution model is extremely sensitive to the duration of the contact event and is best suited for impulse type simulations. It is not optimal for time histories that include a large number of contact events in which the force vector is not known beforehand.

The stiffness parameter is reasonable for the lightly loaded medium steel pair. The response of interest occurs over a very short time interval, around one hundred milliseconds. Because damping in meshing gears is such a small percentage of the elastic force, its affect on the simulation results is negligible. The penetration d_c is defined as the depth at which the damping force reaches its maximum value, details provided in [10]. Modification of this value does not have a significant effect on the response of either gear.

Table 1. Geometric parameters and simulation contact force

Algorithm		ADAMS impact
Stiffness	K	2 x 10^7 N/mm
Force Exponent	e	2.2
Damping	c	2 x 10^{-2} N-s/mm
Penetration	d_c	1 x 10^{-7} mm
Module	m	1 mm/tooth
Pressure Angle	Φ	20 deg
Face Width	F	10 mm
Pinion	Z_p	20 teeth
Gear	Z_g	80 teeth
Backlash	B	0.05 mm

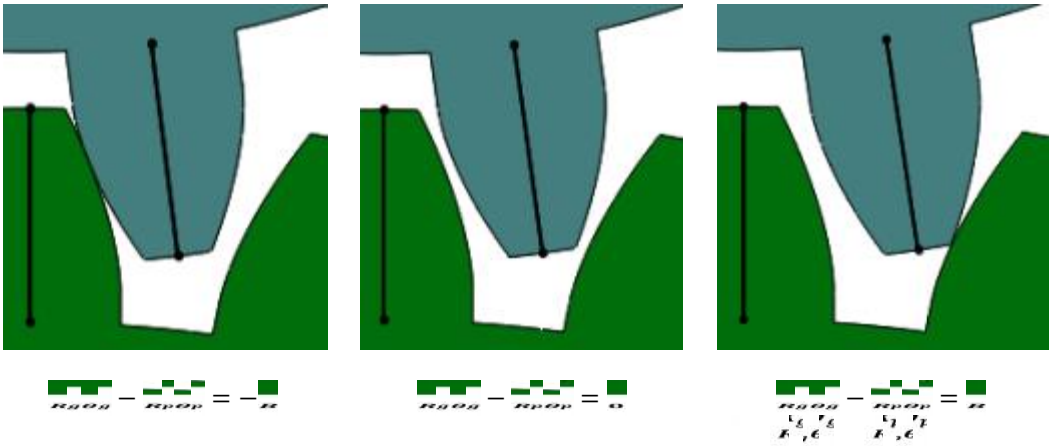

Fig.1. Relative displacement along the line of action, $S = R_g\theta_g - R_p\theta_p$

Combined with gear profile errors backlash may cause loss of contact between gear teeth. This may induce consecutive single-sided or double-sided impacts and generate large impact forces with large vibration. R_p and R_g are the radii of the base circles of pinion and gear, respectively. The relative displacement between the two mating teeth profiles along the line of action is represented as, $S = R_g\theta_g - R_p\theta_p$, shown in Fig.1. When S is larger than the gear backlash B, there is contact between pinion and gear. For a fixed axis external spur pair,

$$-B \leq R_g\theta_g - R_p\theta_p \leq B$$

As a reference, the boundary and initial conditions published in [16] are shown in Table 2. The results produced by the multi-body kinematic model are in very close agreement to the published results, shown in Fig.2 - Fig.4. This analytical formulation accurately captures the dynamic forces and behavior of the mechanical transmission system and can be applied to the more complicated planetary gear.

Table 2. Dynamic conditions depicted in Fig.2 - Fig.4

Case	Simulation parameters
1	ω_{p0} = 50 rad/s initial angular velocity applied to the pinion

2	ω_{p0} = 50 rad/s initial angular velocity applied to the pinion T_p = 35 N-mm constant torque applied to the pinion T_g = -35 N-mm constant torque applied to the gear
3	T_p = 100sin(1000t) N-mm sinusoidal torque applied to the pinion

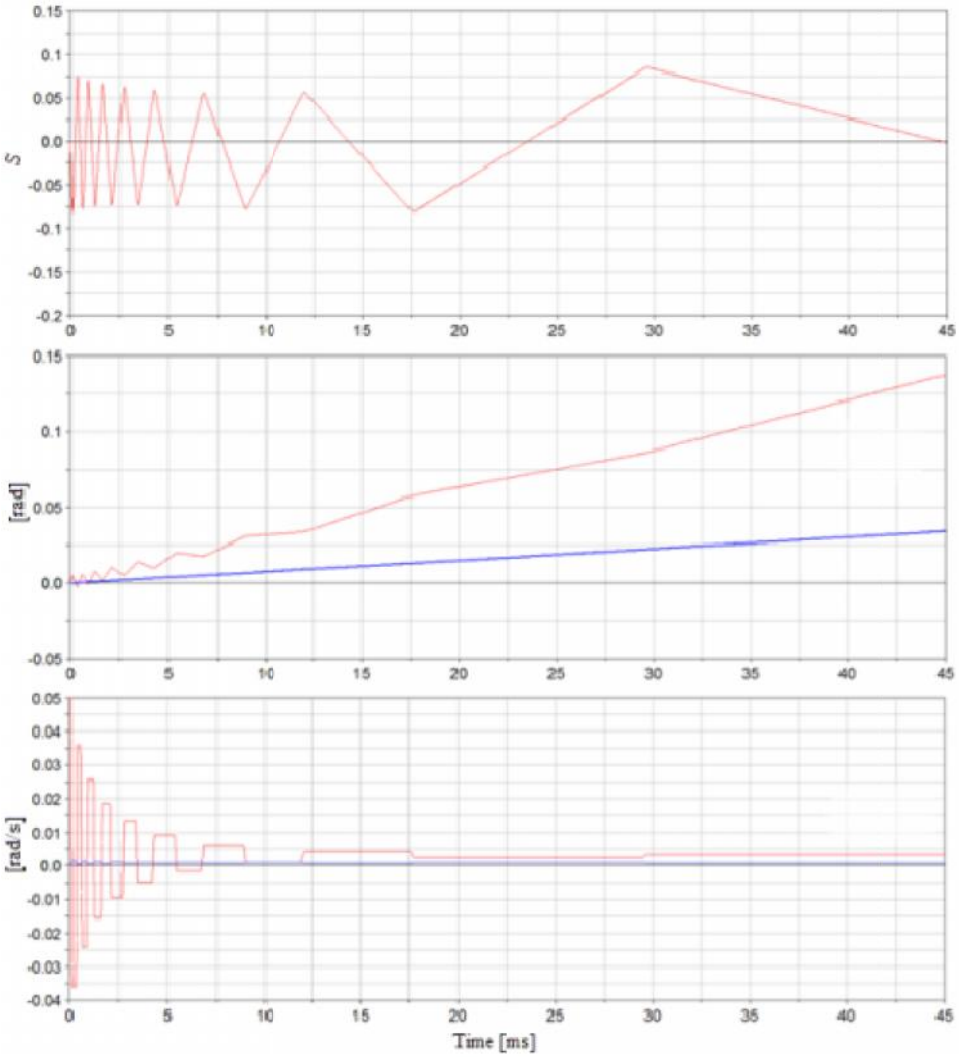

Fig.2. Case 1 results are in close agreement with reference [16] Fig8(a,b,c)

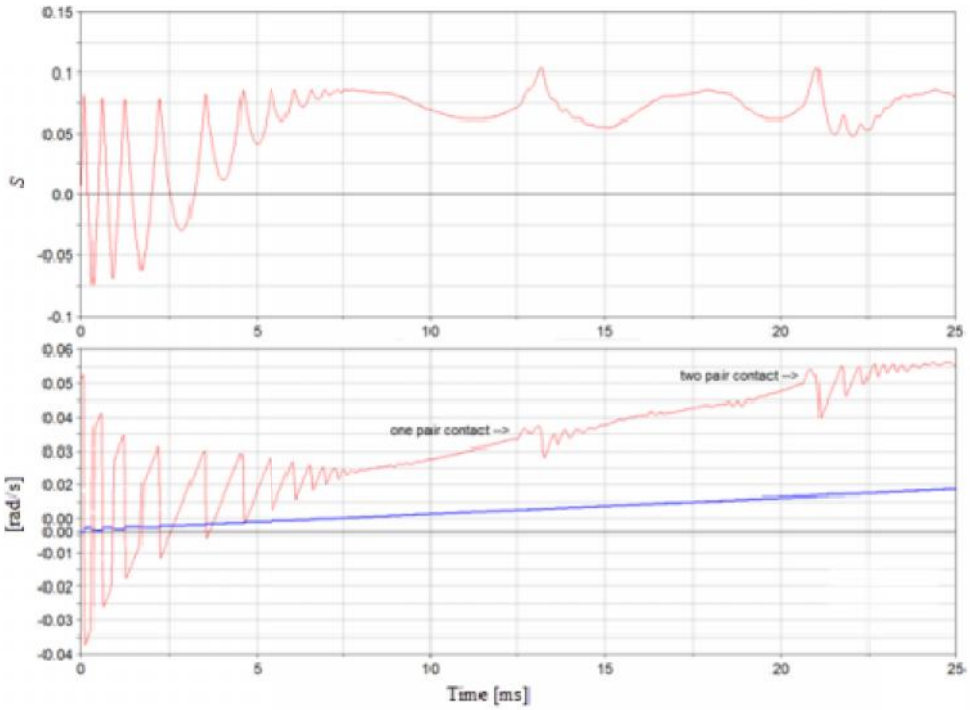

Fig.3. Case 2 results are in close agreement with reference [16] Fig9(a,b)

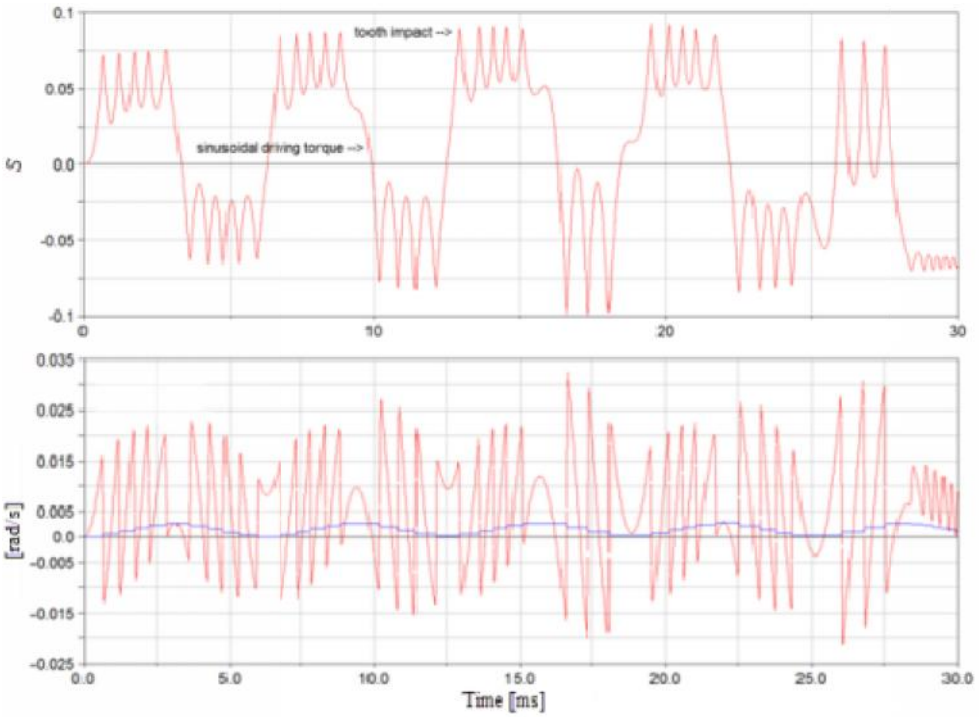

Fig.4. Case 3 results are in close agreement with reference [16] Fig10(a,b)

3. Modeling a differential planetary gear train with backlash and teeth damage

The differential planetary gear chosen for study has two inputs and one output [11,12,13]. The system schematic and CAD model are shown in Fig.5(a), and Fig.5(b), respectively. The profile of the chipped sun gear tooth is shown in Fig 6. Geometric design parameters of this planetary transmission are calculated in Table 3. The multi-body kinematic model formulation is defined in the same manner as in Section 1. As a reference, the dynamic conditions presented in the Figures are shown in Table 4.

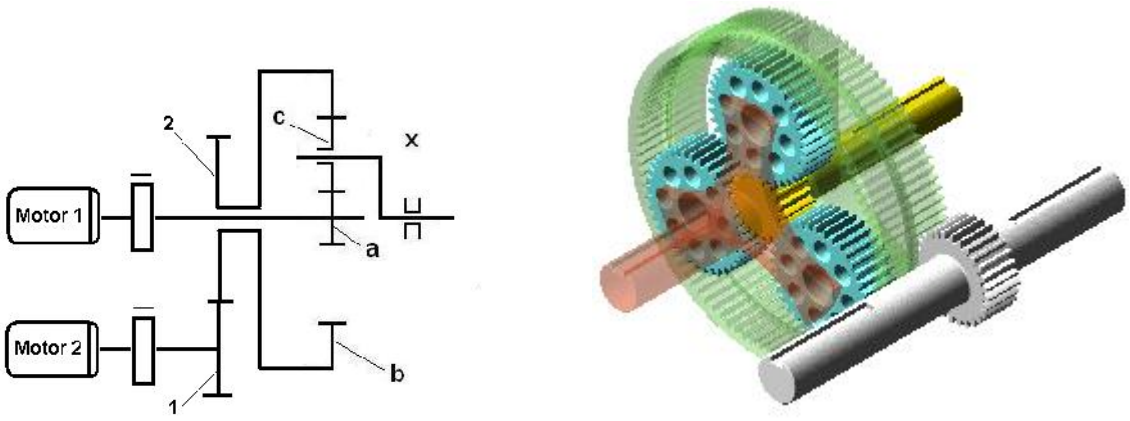

(a) Schematic **(b) CAD model**

Fig.5. A differential planetary gear with two inputs and one output, the ring has both internal and external teeth

Table 3. Design and simulation parameters

Number of teeth	Z_a=20; Z_b = 94 Z_c= 37; Z_1 =28 Z_2 = 98	Material properties	E = 2.07 x 10^{11} Pa; ν = 0.29; ρ = 7801 kg/m^3
Pitch diameter mm	D_a= 40; D_b = 188 D_c=74; D_1 =56 D_2 = 196	Force exponent	2.2
Module	2	Backlash	B_1 = 0.04 mm B_2 = 0.03 mm
Gearing ratios	5.7; 1.213	Penetration	10^{-7} mm
Pressure angle	20º	Stiffness	2 x 10^7 N/mm

Table 4. Dynamic conditions depicted in the Figures

Fig. No.	Simulation Parameters
31, 32	ω_{x0} = 100 rad/s initial angular velocity applied to the carrier, fixed ring
33, 34, 35	ω_{x0} = 100 rad/s initial angular velocity applied to the carrier, free ring
36, 37, 38	ω_1 = 102.1 rad/s constant angular velocity applied to the sun, fixed ring
39, 40, 41(a)	T_1 = 70.5 N-m step torque applied to the sun, fixed ring
41(b), 42	T_1 = 70.5 N-m step torque applied to the sun, T_2 = 67.9 N-m applied to gear 1

Fig.6. Chipped tooth profile

4. Dynamic response and discussion of a planetary gear with constant velocity and applied step torque to the sun

The ring is held fixed and the sun is being driven by Motor 1 which has a constant angular speed of 102.1 rad/s = 975 rpm. The planet gears must be rotating in a direction opposite that of the sun and carrier for the engagement to be dynamically feasible. During the first few milliseconds the angular velocities change rapidly, then converge to an average speed consistent with their respective gearing ratios. The planet inertia is much smaller than the carrier assembly. Since the planets experience forces from the sun and internal ring, their angular velocities have a larger change in amplitude. These oscillations reduce quickly because the system is being driven by the kinematic constraint of a constant angular speed, which defines angular velocity ω as a function of time, ω = ω(t). Therefore, the sun will have the prescribed motion regardless of any force it experiences, causing the system to reach steady-state rapidly.

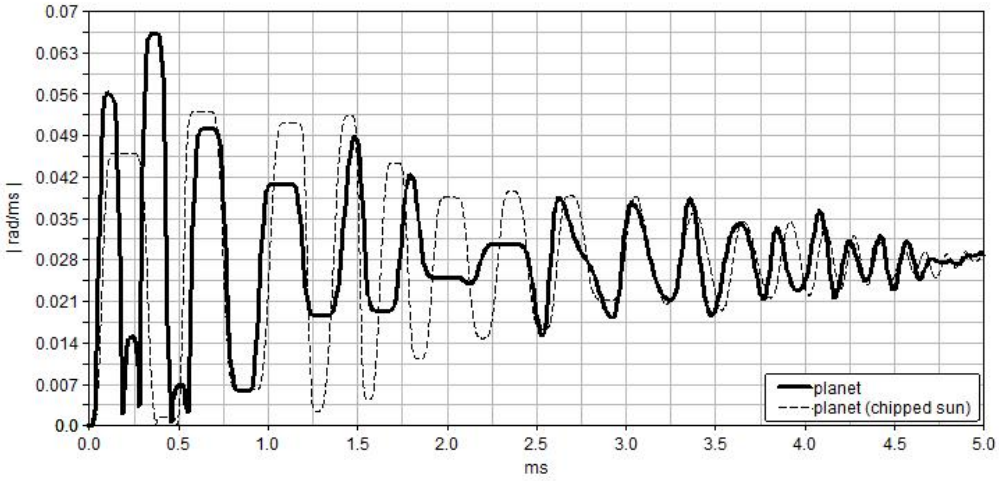

Fig.7. Angular velocities when constant angular velocity ω_1 = 102.1 rad/s is applied to the sun

Consideration of a sun with a chipped tooth is shown in Fig.7. Between 1 and 3 ms the magnitude of the angular velocity has increased. This is because the planet has more room to move in the larger backlash induced by the damaged tooth. An impact force causes a change in angular acceleration which propagates further because of the profile gap. The response of the perfect involutes and chipped planets become nearly identical after 10 ms because the damaged tooth has moved through the engagement cycle.

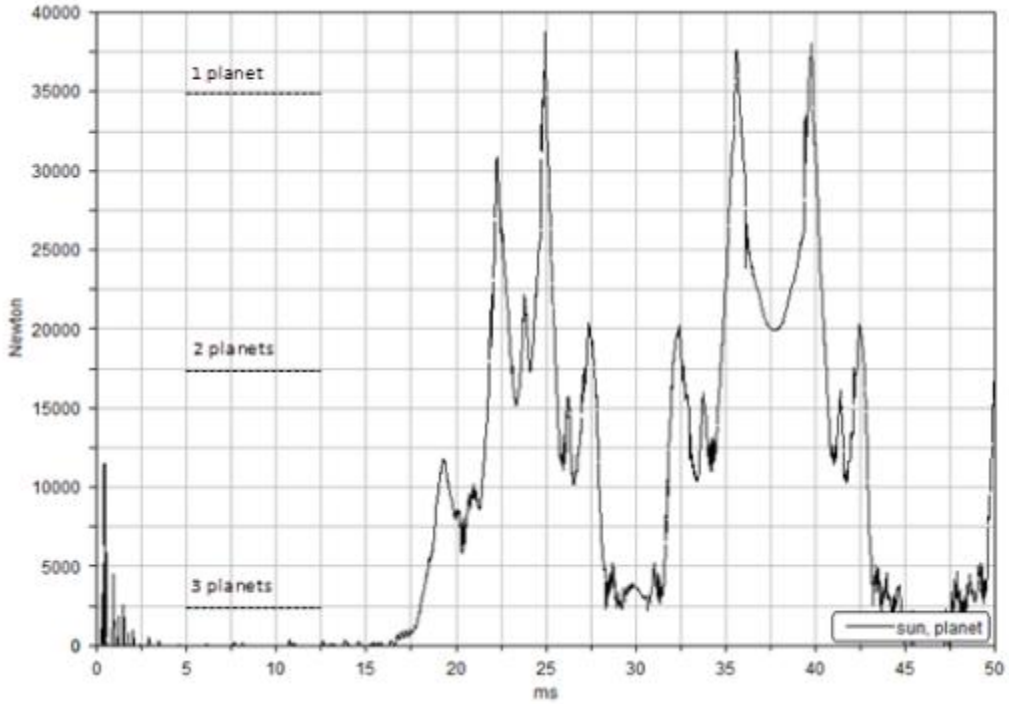

Fig.8. Sun-planet contact force when the torque T_1 = 70.5 N-m is applied to the sun

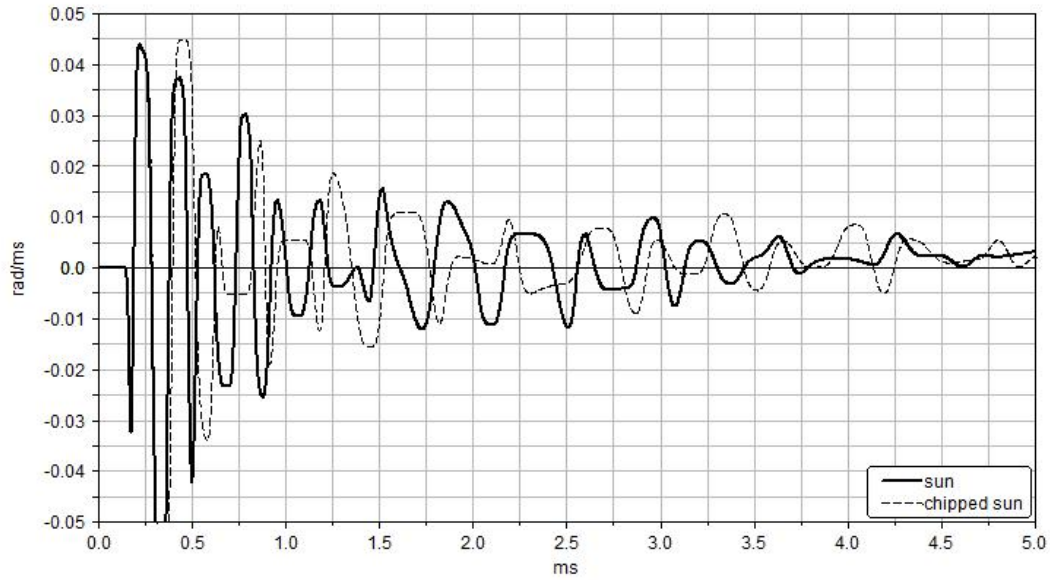

Fig.9. Sun angular velocity when the torque T_1 = 70.5 N-m is applied to the sun

With a fixed ring, a realistic step torque of the form $T(1 - e^{t/\tau})$ is applied to the sun input shaft to represent an electric motor, with magnitude and time constant derived from rated operating conditions. The first large magnitude occurs at 9 ms for constant input speed, while the same magnitude in Fig.8 does not occur until 25 ms. An applied torque creates an angular acceleration which acts against the resistive inertia of the sun. This causes the force response to become delayed relative to the constant speed case. The largest magnitudes occur when this planet is the only planet in contact with the sun. The smaller magnitudes are due to the load sharing resulting from the dynamic sun contact ratio. The chipped sun experiences fewer

impact events than the sun with standard involute profiles, shown in Fig.9. It takes longer for the gears to contact due to the damaged tooth. The chipped sun experiences larger velocity changes because the torque has accelerated the sun for a longer time before contact. These velocity changes create large force magnitudes. The oscillations dissipate quickly as the system accelerates and contact between gear teeth becomes constant along one side only. Velocity changes from positive to negative, like those shown in Fig.9, represent double-sided impacts induced by torsional vibration.

5. Dynamic response and discussion of a planetary gear with a step torque applied to both the sun and gear 1

The system is operating in differential mode with Motor 1 and Motor 2 operating in the same direction. A step torque of the form $T(1 - e^{t/\tau})$ is applied to both the sun and gear 1 to represent an electric motor, with the magnitude and time constant derived from rated operating conditions. With a fixed ring as in Fig.10 (a), the sun exhibits the form of the step function used to model the input torque. The sun oscillates with the largest amplitude because it has the smallest inertia. The planets dissipate energy from the sun input to the carrier output. The three planets must accelerate the carrier's large inertia from rest. The amplitude of the sun's velocity change is reduced with the system operating as a differential transmission, shown in Fig.10(b). Operating in the differential mode the ring and carrier move in the same direction as the applied torque on the sun. This makes the magnitude of the sun's angular velocity change more smooth compared to the simple planetary configuration with a fixed ring. The same effect is seen in the other elements. The detrimental effects of the sun's chipped tooth are reduced with the system operating in the differential mode.

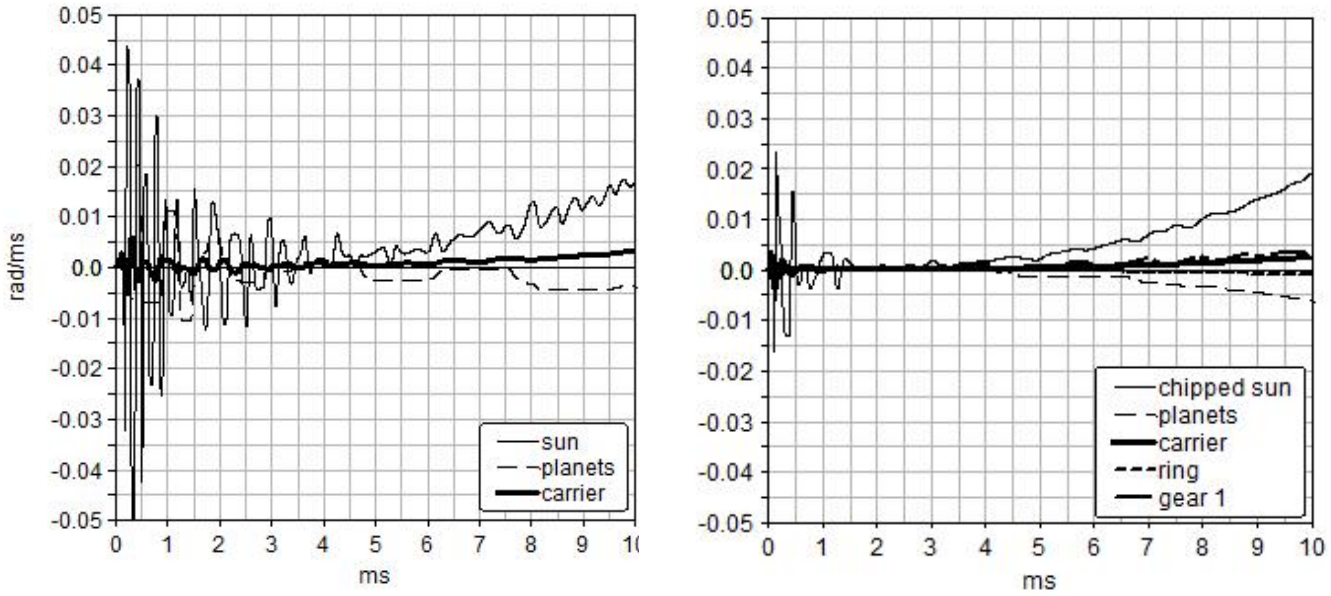

(a) Fixed ring, T_1 = 70.5 N-m **(b) Free ring, T_1 = 70.5 N-m, T_2 = 67.9 N-m**

Fig.10. Angular velocity with applied step torques

The mesh between gear 1 and ring has a smaller prescribed backlash than the sun and planet meshes. Therefore, contact occurs in this external fixed axis mesh before the sun and planets. A clear succession of impacts shown in Fig.11. The interval from 3.5 ms to 4.5 ms shows that as gear 1 contacts the ring, the ring contacts a planet, and the planet contacts the sun. The planets can simultaneously be in contact with the sun and ring. This complication means that the force in the fixed axis mesh directly affect the magnitude of the force between a planet and ring, shown as the 10 N peak at 7.5 ms. The dynamic response of the planet is due to a superposition of the impacts in its sun and ring meshes.

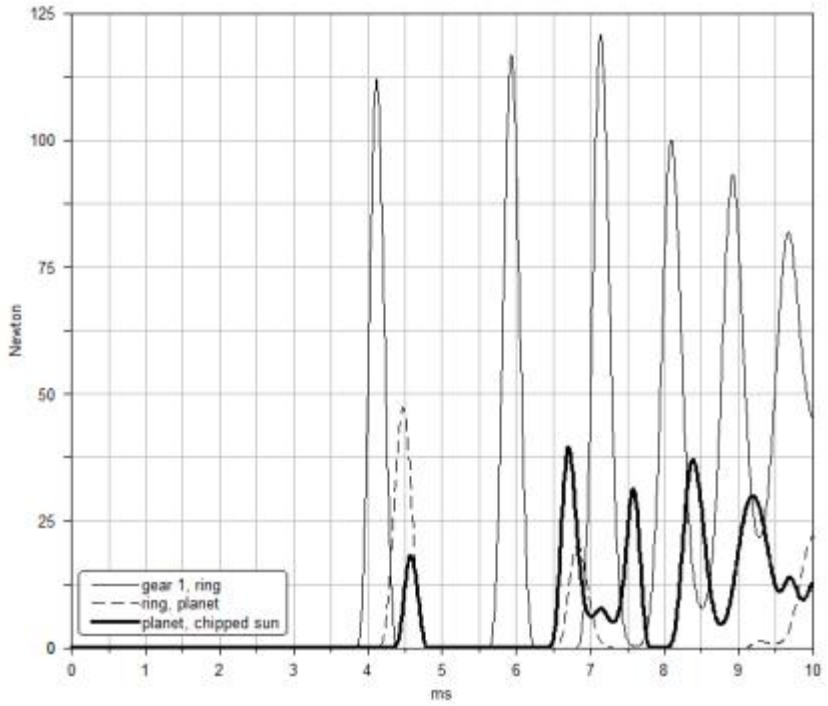

Fig.11. Angular velocity when torque T_1 = 70.5 N-m is applied to the sun and T_2 = 67.9 N-m is applied to gear 1

6. Steady-state frequency domain simulation results and discussion

The system is operating in the differential mode, with Motor 1 and Motor 2 operating in opposite directions. Constant angular velocities of 16.3 Hz = 975 rpm, and -12.4 Hz = 745 rpm, are applied to the sun and gear 1, respectively. A small resistive torque is applied to both the ring and carrier assembly. The value of the resistive torques are around one percent of the element's torque at steady-state. This resistive inertia models the frictional torque generated by the bearings, couplings, and fluid shear of the realistic planetary transmission. For testing purposes, a standard feedback control system can maintain the constant input speed on both shafts.

The predicted spectrum includes harmonics of gear mesh frequencies and element spin speeds. Predicted frequencies up to 1000 Hz are calculated in Table 3. The sun, planet, and internal ring share the same *planetary* gear mesh frequency denoted as GMF_{abc}. The *fixed axis* mesh between gear 1 and the ring (gear 2) is denoted as GMF_{12}. This fixed axis mesh is characterized by a common factor of 14, therefore the n/CF subharmonics are included in the predicted spectrum. The *abc12* naming convention is consistent with the schematic of Fig.3(a). Both the planetary and fixed axis meshes have unique force histories when the transmission is operating in the differential mode, shown in Fig.12 for prescribed backlash and ideal involute profiles.

The fixed axis mesh between gear 1 and gear 2 is independent from the coupled kinematics of the planetary meshes. The largest amplitudes correspond to the gear meshing frequencies. The sidebands in the planetary mesh are modulations of sun spin speed because the sun is driven by Motor 1. Similarly, sidebands in the fixed axis mesh are modulated by the gear 1 spin speed because it is driven by Motor 2. The time and frequency domains of each mesh are shown in Fig.12.

The element spin speeds and their superharmonics are contained in the first 50 Hz of the planetary mesh spectrum, shown in Fig.13(a). The spin speed of the sun has the largest amplitude because the planetary mesh is driven by its constant angular velocity. The impacts in the fixed axis pair are transmitted to the elements in the planetary mesh through the ring. This force propagation causes a reduction in the amplitude of the gear 1 spin speed and its superharmonics when observed from the planetary mesh spectrum. The planetary gear mesh frequency is modulated by the sun spin speed and its subharmonics, shown in Fig.13(b). The sun spin speed subharmonics are a function of the number of planet gears calculated in Table 3. The subharmonics create wide 50 Hz sidebands around the gear mesh frequency. The fixed axis meshing frequency appears in the planetary mesh spectrum when a chipped tooth is included on the sun. The magnitude of the effect is reduced when an eccentric tooth is included on a planet. The fixed axis gear mesh frequency is modulated by the sun spin speed and its

subharmonics although it is not included in the planetary mesh elements. The presence of GMF_{12} in the planetary mesh FFT indicates damage on a sun tooth. This is a potentially new and important vibration signature of the defected gear train.

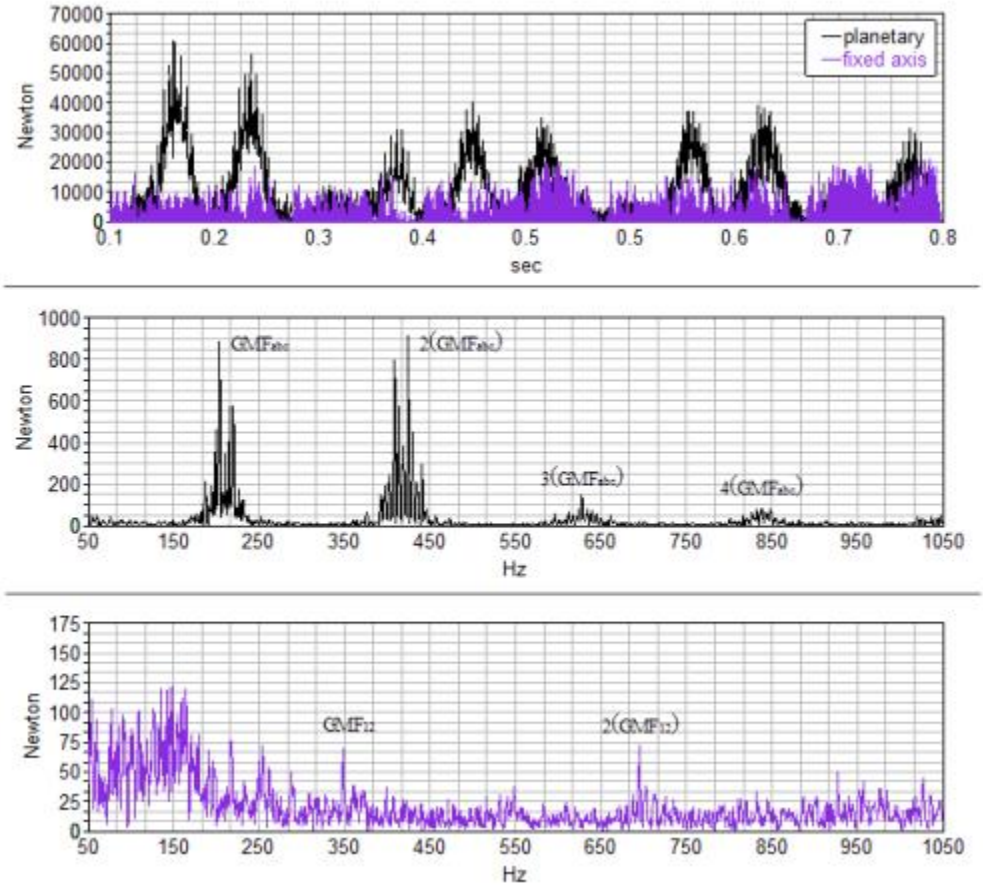

Fig.12. Time and frequency domain representations of force in the planetary and fixed axis meshes

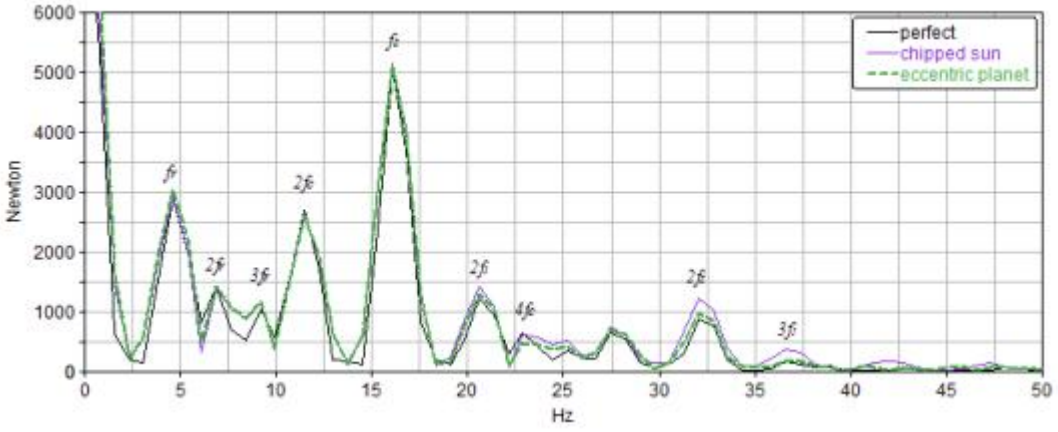

(a)

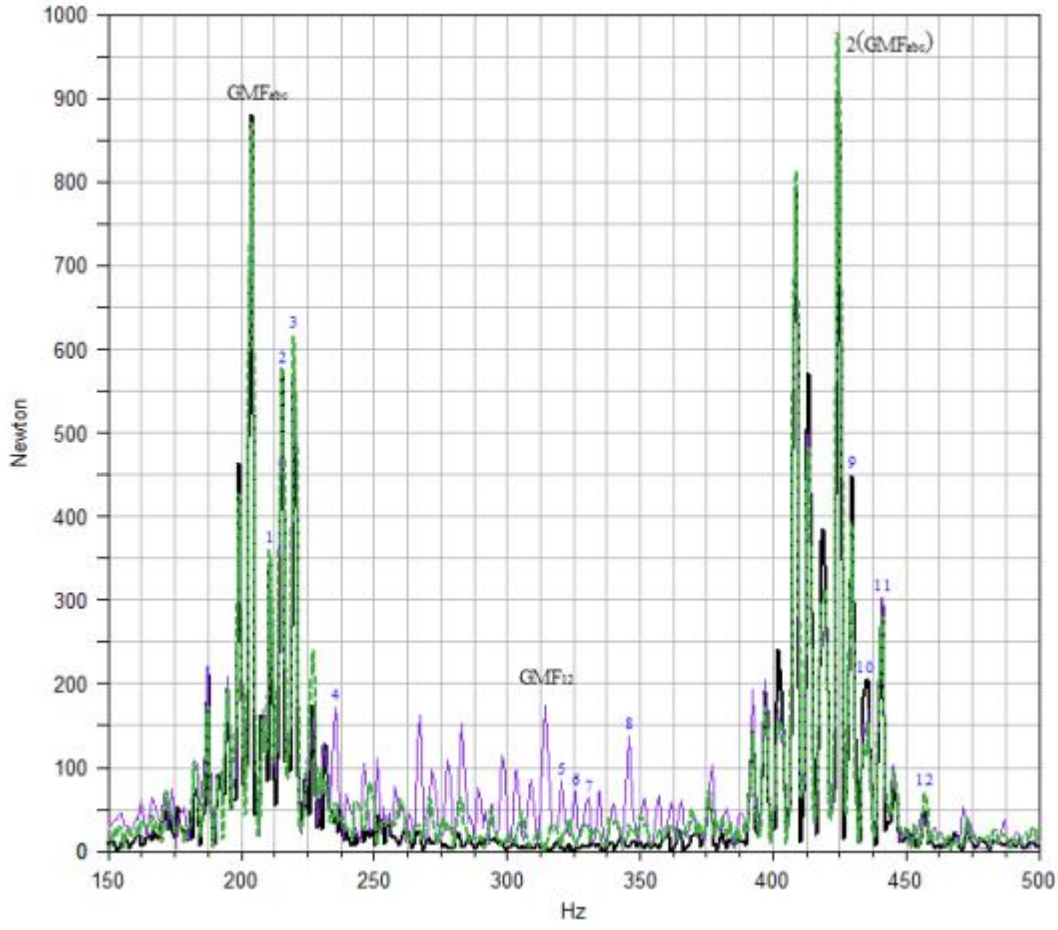

(b)

Fig.13. Force magnitude in planetary mesh elements include (a) spin speed components, and (b) modulated gear mesh frequencies.
See Table 4 for frequency label definitions.

Table 5. Theoretical frequencies for the differential operating mode in Hz

	Frequency		
	1X	2X	3X
GMF_{abc}	209	419	628
GMF_{12}	347	695	1042
1/14	25	50	74
2/14	50	99	149
3/14	74	149	223
4/14	99	199	298
5/14	124	248	372
6/14	149	298	447
7/14	174	347	521
8/14	199	397	596
9/14	223	447	670
10/14	248	496	745
11/14	273	546	819
12/14	298	596	894
13/14	323	645	968
1	347	695	1042

		Spin Speed		
		1X	2X	3X
Ring	f_r	3.6	7.1	10.7
Carrier	f_c	5.8	11.6	17.3
Planet	f_p	6.1	12.3	18.4
Gear 1	f_1	12.4	24.8	37.2
Sun	f_s	16.3	32.5	48.8

Table 6. Frequencies of Fig.9

Sideband	Point	Hz
$GMF_{abc} \pm \frac{1}{3}f_s$	1	215
$GMF_{abc} \pm \frac{2}{3}f_s$	2	221
$GMF_{abc} \pm f_s$	3	226
$GMF_{abc} \pm 2f_s$	4	242
$GMF_{12} \pm \frac{1}{3}f_s$	5	352
$GMF_{12} \pm \frac{2}{3}f_s$	6	358
$GMF_{12} \pm f_s$	7	363
$GMF_{12} \pm 2f_s$	8	380
$2(GMF_{abc}) \pm \frac{1}{3}f_s$	9	424
$2(GMF_{abc}) \pm \frac{2}{3}f_s$	10	430
$2(GMF_{abc}) \pm f_s$	11	435
$2(GMF_{abc}) \pm 2f_s$	12	451

7. Joint time-frequency analysis (JTFA)

In order to demonstrate how the frequency content of force changes with time a joint time-frequency analysis (JTFA) is performed based on transient start-up conditions. Fig.14 is created from the force history between gear 1 and the external teeth of the ring. The fixed axis force vector is chosen for study because of its unique interaction with the ring. The ring makes direct contact with all elements in the transmission except the sun. Therefore, the force vector between gear 1 and the ring contains information about the dynamics of the entire system. An exponential step of the form $\omega(1 - e^{t/\tau})$ is applied to

both the sun and gear 1 to represent a characteristic electric motor. The magnitudes are -78.0 rad/s for gear 1, and 102.1 rad/s for the sun, with $\tau = 1000$ ms. A resistive torque is applied to both the carrier assembly and the ring, with a magnitude around one percent of the element's torque at steady-state. Aliasing issues are prevented by using a large number of integration steps and a long simulation duration of 4 seconds. Spectrum leakage is reduced by overlapping a sliding time sample of 100 ms by 98% and applying a Hamming window to each sample.

Due to the nonlinearity caused by the interaction of the damaged tooth and different backlash, a large number of contact events are created which occur at nearly random intervals. The random nature of the impacts produces a frequency domain with some noise. The low amplitude peaks observed between 1250 Hz and 1450 Hz continue until approximately 5000 Hz, with frequencies greater than 5000 Hz near zero. At 760 ms the second harmonic of the *fixed axis* gear mesh GMF_{12} is identified as the largest peak at 650 Hz. This value is less than the 695 Hz listed in Table 3 because the system has not accelerated to its full operating speed at $\tau = 1000$ ms. The 3X(sun) speed is a strong excitation because of the chipped sun tooth. The damaged tooth rotates through a planet mesh three times per revolution. Therefore, the 3X(sun) speed is not a harmonic but rather the fundamental excitation of the chipped sun. The four largest peaks along the 760 ms line are modulated by the 3X(sun) frequency. The second harmonic of $2(GMF_{12})$ dominates the spectrum through the 650 to 1000 ms range with sidebands also equal to 3X(sun). The sidebands increase in frequency along with system speed to their final value of 48.8 Hz at 1000 ms. An increase in the separation between peaks is observed. Along the 1000 ms line the third harmonic of $3(GMF_{12}) = 1042$ Hz is present with sidebands of 3X(sun). The fourth harmonic of $4(GMF_{abc}) = 838$ Hz falls in this region with magnitudes comparable to the GMF_{12} harmonics. It notable that the fundamental GMF_{12}, GMF_{abc}, and $2(GMF_{abc})$ are not the dominant frequencies during start-up.

The curvature in the spectral lines in the time domain is due to the acceleration of the ring. As the system accelerates from rest, the first contacts occur from gear 1 to the ring, and from the sun to each planet. The ring and planets oscillate within their backlash at high frequency because velocity is not prescribed on these elements. The ring accelerates away from the direction of contact up to 350 Hz, causing the contacts with gear 1 and the planets to occur at increasingly longer intervals. The ring's acceleration away from the direction of contact causes the frequency of all spectral lines to decrease. The opposite occurs during the interval of 350 ms to 450 ms. Here the ring decelerates slightly, decreasing the interval between contacts and causing an increase in spectral frequency. The magnitude of oscillation in the ring's acceleration diminishes with time with all spectral lines remaining straight for $t > \tau$.

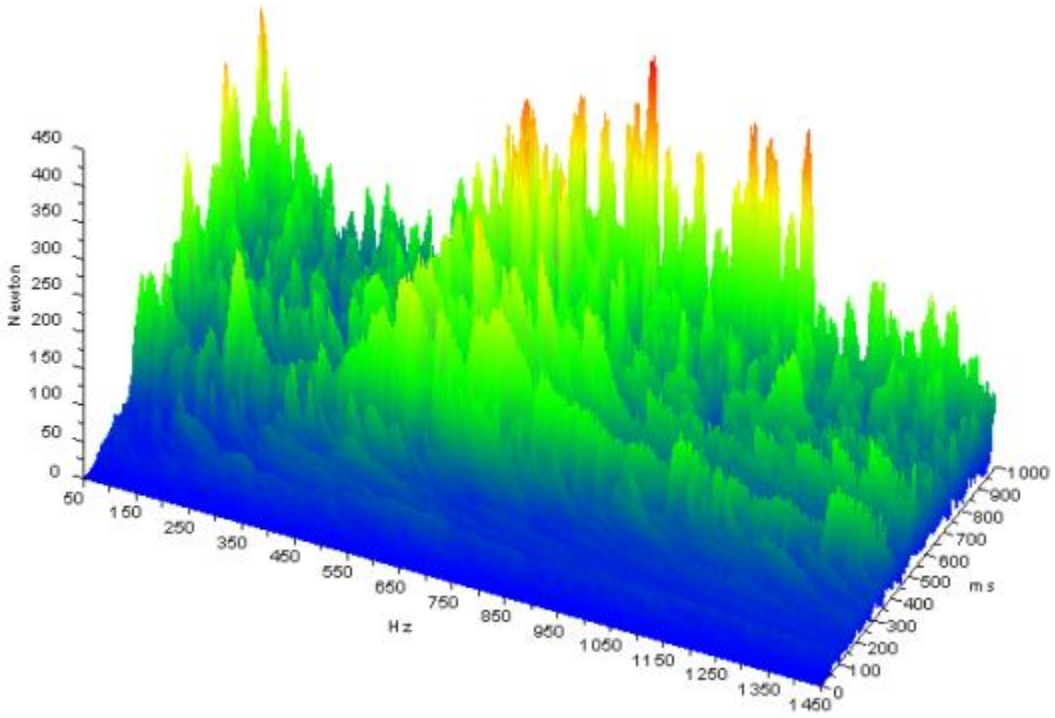

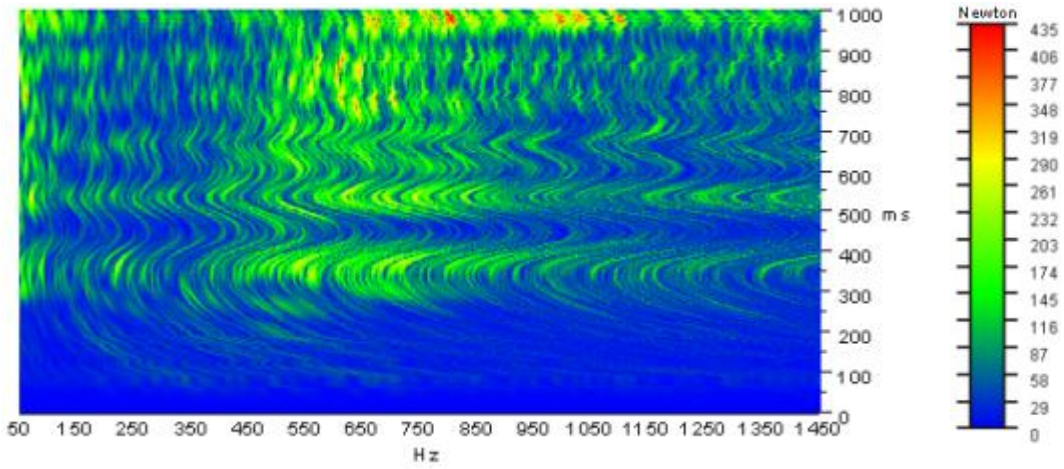

Fig.14. Three dimensional FFT of force magnitude in the fixed axis mesh for prescribed backlash and chipped sun with an exponential step angular velocity on both sun and gear 1

8. Conclusions

A practical differential planetary gear train which combines two inputs and one output has been investigated using a non-linear multi-body dynamics model. To avoid interference and undercut the backlash between the sun-planet and planet-ring meshes are precisely defined. When the transmission operates with a fixed ring and undergoes free vibration from a near symmetrical position, six contact forces are potentially active. The magnitude of the contact forces depend on the time varying contact ratios of each element. The duration of the contact event decreases with a freely rotating ring and applied initial velocity.

Step torques of opposite directions to each input shaft closely model the constraints and loading conditions of realistic operation. The dynamics of the differential mode are shown to be less destructive to the sun. The characteristics observed in the time and frequency domains are due to the interaction of many components of the differential planetary transmission. Fast Fourier Transform (FFT) analysis shows harmonics of the gear mesh frequency with varying sideband modulation. A joint time-frequency analysis (JTFA) during start-up reveals unique vibration patterns when the contact forces increase during acceleration.

9. REFERENCES

1. Özgüven H.N. and Houser D.R., "Mathematical Models used in Gear Dynamics – A Review", *Journal of Sound and Vibration*, 121(3), 1988, pp. 383-411.

2. Parey, A. and Tandon, N., "Spur Gear Dynamic Models Including Defects: A Review", *The Shock and Vibration Digest,* Vol. 35, No. 6, Nov. 2003; pp. 465-478.

3. Parey, M. El Badaoui, F. Guillet, N. Tandon, "Dynamic modeling of spur gear pair and application of empirical mode decomposition-based statistical analysis for early detection of localized tooth defect", *Journal of Sound and Vibration* Vol. 294, 2006, pp. 547–561.

4. J. Lin and R. G. Parker, "Parametric Instability of Planetary Gears under Mesh Stiffness Variation**",** *Journal of Sound and Vibration***,** 2002, vol. 249, pp. 129-145.

5. J. Lin and R. G. Parker, "Analytical Characterization of the Unique Properties of Planetary Gear Free Vibration**",** *ASME Journal of Vibration and Acoustics*, vol. 121, July 1999, pp. 316-321.

6. Yi Guo and R. G. Parker, "Dynamic Modeling and Analysis of a Spur Planetary Gear Involving Tooth Wedging and Bearing Clearance Nonlinearity**",** *European Journal of Mechanics A/Solids*, 2010, vol. 29, pp. 1022-1033.

7. R. G. Parker and X. Wu, "Vibration Modes of Planetary Gears with Unequally Spaced Planets and an Elastic Ring Gear**",** *Journal of Sound and Vibration*, 2010, vol. 329, pp. 2265-2275.

8. Yichao Guo and R. G. Parker, “Purely Rotational Model and Vibration Modes of Compound Planetary Gears”, *Mechanism and Machine Theory*, 2010, vol. 45, pp. 365–377.

9. Kong, D., Meagher, J., Xu, C., Wu, X., Wu, Y., “Nonlinear Contact Analysis of Gear Teeth for Malfunction Diagnostics”, *IMAC XXVI a Conference on Structural Dynamics*, Society for Experimental Mechanics, Orlando, Florida USA, February 4 –7, 2008.

10. MSC Inc., *MSC ADAMS reference manual*.

11. Raymond J. Drago, “Fundamentals of Gear Design”, 1988.

12. Huamin Li, Guixian Li, “Gear Mechanism Design and Application”, 2007 (in Chinese).

13. Zengang Rao, “Planetary Gear Transmission Design”, 2003 (in Chinese).

14. Sommer, A., Meagher, J., Wu, X., “Gear Defect Modeling of a Multiple-Stage Gear Train”, Modelling and Simulation in Engineering, Volume 2011 (2011), Article ID 754257, 8 pages

15. Wu, X., Meagher, J., Sommer, A., “A Differential Planetary Gear Model with Backlash and Teeth Damage”, IMAC XXIX a Conference and Exposition on Structural Dynamics, Society for Experimental Mechanics, Jacksonville, Florida USA, Jan. 31 – Feb. 3, 2011.

16. Kuang, J. H., and Yang, Y.T., "An Estimate of Mesh Stiffness and Load Sharing Ratio of A Spur Gear Pair," in *Proceedings of the ASME 12th International Power Transmission and Gearing Conference*, Scottsdale, Arizona, DE-43, 1-10, 1992.